JOURNAL OF SOLID STATE CHEMISTRY 1, 536–544 (1970)

Mixed Oxides of the Type MO_2 (Fluorite)-M_2O_3. IV. Crystal Structures of the High- and Low-Temperature Forms of $Zr_3Yb_4O_{12}$†‡

M. R. THORNBER

Division of Applied Mineralogy, C.S.I.R.O., Wembley, Western Australia

AND

D. J. M. BEVAN

School of Physical Sciences, The Flinders University of South Australia, Bedford Park, South Australia

Received September 15, 1969

The structures of the high- and low-temperature forms of the phase $Zr_3Yb_4O_{12}$ have been determined from single crystal X-ray studies. Both structures are derived from the cubic fluorite type MO_2 by ordered omission of oxygen atoms along one cubic [111] direction and a corresponding rhombohedral distortion to give $R\bar{3}$ space group symmetry. The major difference between the two forms is shown to be due to partial ordering of the metal lattice in the low-temperature form as compared with a random occupancy of Zr and Yb atoms on the metal sites for the high-temperature form. The details of these two structures are discussed in conjunction with the known structures of similar compounds.

Introduction

The general reappraisal of the nature of grossly nonstoichiometric phases, which has taken place over the last ten to fifteen years and in which Wadsley was deeply involved, has produced ever-mounting evidence to show that a description in terms of a random distribution of point defects is no longer adequate. Instead, there has developed the concept that a nonstoichiometric phase at equilibrium is microheterogeneous in character, that it is a fluctuating system which, on time-average, consists of small regions or microdomains differing in *structure* and *composition* from the matrix but dispersed in and coherent with it (*4*), (*5*), (*6*), and (*7*).

† Part I. Oxygen Dissociation Pressures and Phase Relationships in the System CeO_2–Ce_2O_3 at High Temperatures (*1*).

Part II. Non-Stoichiometry in Ternary Rare-Earth Oxide Systems:

A. The System CeO_2–Y_2O_3.

B. The Systems CeO_2–M_2O_3 (M = La,Nd,Sm,Gd,Dy,Ho,Yb) (*2*).

Part III. Crystal Structures of the Intermediate Phases $Zr_5Sc_2O_{13}$ and $Zr_3Sc_4O_{12}$ (*3*).

‡ This work was carried out in the School of Chemistry, University of Western Australia.

Grossly nonstoichiometric fluorite-related phases have long been known to occur in pseudobinary systems of the type MO_2(fluorite)-$M_2'O_3$ (M′ = rare-earth, Y, Sc); they also occur at high temperatures in true binary systems of this type, e.g., PrO_2–Pr_2O_3 (*8*), although at low temperatures in these systems there exists a homologous series of intermediate stoichiometric phases whose general formula is M_nO_{2n-2}. As has been stated (*3*), it is important to know the structures of the intermediate phases if the nature of the short-range order existing at high temperature, which the microdomain concept implies, is to be understood. Any structural feature common to the series of fully-ordered intermediate phases is likely to persist at high temperatures in the nonstoichiometric phase.

In this context the structures of the intermediate phases $Zr_3Sc_4O_{12}(\delta)$ and $Zr_5Sc_2O_{13}(\gamma)$ occurring in the system ZrO_2–Sc_2O_3 were determined previously (*3*). The common structural feature found in this work is shown in Fig. 1 as an idealized model emphasizing the close relationship to the fluorite structure (MO_8 cubes sharing edges). The black cube is in fact MO_6V_2 (V is a *vacancy* in the fluorite lattice), and these vacancies are at each end of that body-diagonal of the MO_8 fluorite cube which

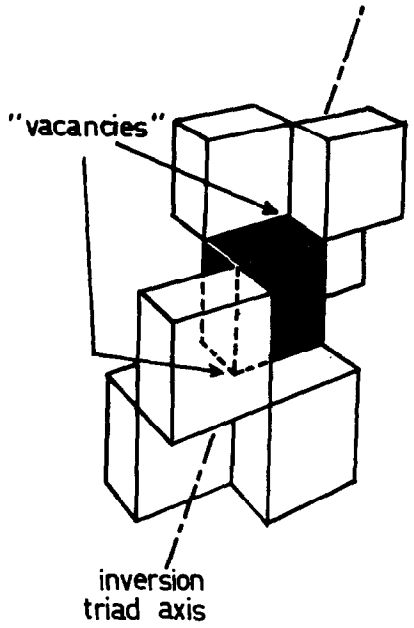

FIG. 1. Defect complex consisting of a central 6-coordinated metal atom surrounded by six 7-coordinated metal atoms.

becomes the unique inversion triad of the new structures. The white cubes are MO_7V, and the whole is an element of the M_7O_{12} structure. This paper reports new structural results on the phase $Zr_3Yb_4O_{12}$, which exists in both a high- and low-temperature form. The succeeding paper describes studies of phase relationships in the system ZrO_2–M_2O_3 (M = Sc, Yb, Er, Dy), and interprets the results in the light of structural information obtained from intermediate phases.

Preparation and Structure Determination

The low-temperature form of $Zr_3Yb_4O_{12}$ is identical with the phase prepared by Perez y Jorba (*9*): the high-temperature form has not previously been reported. It was made in an argon-arc furnace: the metal oxides, mixed in the correct proportions either physically or by a coprecipitation method, were melted and then cooled rapidly on the water-cooled copper hearth. The low-temperature form was prepared either by reaction of the oxide mixture at a temperature of about 1600°C, or by subsequent annealing of the quenched melt at 1600°C for several days, after which the temperature was reduced gradually to 1000°C over 7 days.

Both primitive unit cells are rhombohedral. The most marked difference between the high- and low-temperature forms is the greater rhombohedral distortion of the latter; the former is only slightly distorted from cubic. The triply-primitive hexagonal cell dimensions of the two forms are:

high-temperature form
$a = 9.68\ (3)$ Å $\quad c = 8.96\ (7)$ Å,

low-temperature form
$a = 9.65\ (5)$ Å $\quad c = 9.02\ (1)$ Å.

A careful search of melted samples, both annealed and unannealed, with the aid of a polarizing microscope gave some crystal fragments which showed complete extinction when the microscope stage was rotated. However, those fragments used for the structure determinations were quite irregular so that no corrections for absorption could be applied. In view of the high linear absorption coefficient of 976 cm^{-1} for Cu radiation, absorption effects are probably large. Moreover, the crystals were of poor quality in that the diffraction spots showed considerable broadening.

Crystals were mounted with their fast optic axis as the rotation axis because this had been established to be the hexagonal *c* direction. Obverse hexagonal settings were used throughout.

Inclined beam oscillation data were collected on Ilford Industrial-G X-ray film with a Nonius Weissenberg camera and nickel-filtered CuK_α radiation. Overlapping 20° oscillations were used to give a 60° section of reciprocal space.

Intensity data for the low-temperature phase were measured along the lines of constant *l* with a Joyce Lobel microdensitometer. Peak heights were measured, and a correlation made between two tripacks of differing exposure times. This method was not entirely satisfactory because of extreme difficulty in keeping the microdensitometer trace exactly along the centre of the line of spots. This became especially difficult for the weakly-exposed films where the rows of spots were hardly visible. In view of the complications with the microdensitometry, the intensity measurements for the high-temperature phase were made by visual techniques. Intensities were measured for both *+ve* and *−ve* values of *l*, and from the upper and lower halves of the film so that data for many symmetrically identical reflections were collected for correlation purposes. Correction was made for $\alpha_1\alpha_2$ splitting by the method of Barker and Rae (*10*).

Identification and indexing of the inclined beam pattern was carried out with the aid of the inclined beam oscillation indexer "IBOI" program written for the PDP6 computer by Figgis (*11*). The program for Lorentz and polarization corrections [Figgis (*11*)]

was modified slightly in that, after the corrections were made, the indices were permuted trigonally so that they were written onto dectape with l positive and h and k both having the same sign. Correlation between oscillation ranges was thus made easy because there were many reflections common to all the oscillation ranges. The inclined beam oscillation data correlation program [Figgis (*11*)] was used, with any one of the ranges acting as the common range. In order to have the data sorted into the correct order for Fourier summation, and in the required format for analysis, a special program was written. This allowed the intensities of common reflections to be averaged and trigonal permutation of the indices to be made so that the Fourier density maps would maintain proper symmetry.

Powder data were also collected for the low-temperature phase in a manner similar to that described in a previous publication for the γ and δ phases of the ZrO_2–$ScO_{1.5}$ system (*3*). This was at a time when single crystals were not available. These data were fully corrected for all effects including absorption. Structure analysis was carried out on these data by the method described previously (*3*). The result of this analysis was in fact checked by the later analysis of the single crystal data. Because of the absence of mirror and glide planes in the $R\bar{3}$ space group, to which both these structures belong, each powder line of general index, hkl, had a contribution from more than one nonidentical set of planes. The total intensity of the powder lines was allocated between the constituent reflections in proportion to the structure factors calculated as the refinement progressed.

A third set of data was also prepared. Here the intensities of the powder lines were allocated between the constituent reflections which superimpose on the powder pattern in accordance with the single crystal data. The results for the three sets of data were, within the limits of error, identical. The single crystal data suffered from extinction and absorption effects which did not allow proper refinement of temperature factors, and thus the results for the previously mentioned set of data are probably the most reliable because absorption effects have been accounted for, and yet the powder intensity allocation is in no way influenced by the model structure being refined.

Structure analysis for the high-temperature phase was performed on the single crystal data only.

Refinement of both structures was carried out in the $R\bar{3}$ space group with 36 oxygen atoms and 18 averaged Zr–Yb metal atoms in positions 18(f), and 3 averaged Zr–Yb metal atoms in position 3(a), of the hexagonal representation. The initial parameters chosen were those for all atoms in their ideal fluorite position. The full-matrix least-squares program [Busing, Martin, and Levey (*12*)] were used in conjunction with Fourier techniques. Tests were made for metal-ordering and noncentrosymmetry for both structures, but all were rejected except for the final result shown for the low-temperature phase. Refinement in the noncentrosymmetric space group $R3$ gave an increased R factor, a result that was very near to centrosymmetric, and large correlations between the parameters of the centrosymmetrically related atoms. Partial metal-ordering for the low-temperature phase was obtained by allowing refinement of occupancy factors for the metal atoms. The refinement was also in accord with indications from electron density maps.

This result was tested from two approaches:

(i) Random Zr and Yb on all sites
(ii) Zr only occupying the special metal site

and the remaining Zr and Yb atoms occupying the general site at random. Difference Fourier electron density maps and occupancy refinement from both situations gave the same result, in accord with that obtained previously from the powder data by Fourier methods. There is no provision in the block diagonal least squares program used for the powder data for occupancy refinement, so trial and error methods were used in conjunction with Fourier information.

This same test, made on the high-temperature phase data, showed only a marginal tendency for Zr atoms to be preferred in the special position. While this effect makes sense chemically the extent of the change was of no consequence when compared with the standard deviation. The parameters listed in Table I gave

$$R\left(=\frac{\sum||F_o|-|F_c||}{\sum|F_c|}\right)$$

factors of 0.132 (low-temperature form) and 0.168 (high-temperature form) for the respective comparison of calculated and measured structure factors as listed in Tables II and III.

Discussion of Structures

Table IV lists the bond lengths and angles for the $\delta(M_7O_{12})$ phases $Zr_3Sc_4O_{12}$ (*3*), $Zr_3Yb_4O_{12}$ (high-temperature form), $Zr_3Yb_4O_{12}$ (low-temperature form), UY_6O_{12} (*13*), ULu_6O_{12} (*13*), and the

TABLE I

FINAL ATOM POSITIONS

$Zr_3Yb_4O_{12}$ HIGH-TEMPERATURE FORM				
	Metal (1)	Metal (2)	Oxygen (1)	Oxygen (2)
Position	3a	18f	18f	18f
Occupying atom	(ZrYb)	(ZrYb)	O	O
x	0.0	0.2130	0.205	0.180
$\sigma(x)$	0.0	0.0003	0.004	0.005
y	0.0	0.2567	0.021	0.205
$\sigma(y)$	0.0	0.0003	0.004	0.005
z	0.0	0.3516	0.381	0.098
$\sigma(z)$	0.0	0.0006	0.007	0.009
B	0.0	0.0	0.0	0.0
$\sigma(B)$	—	—	—	—
$Zr_3Yb_4O_{12}$ LOW-TEMPERATURE FORM				
	Metal (1)	Metal (2)	Oxygen (1)	Oxygen (2)
Position	3a	18f	18f	18f
Occupying atom	Zr:Yb = 3:1	Zr:Yb = 3.5	O	O
x	0.0	0.2126	0.163	0.217
$\sigma(x)$	0.0	0.0004	0.004	0.004
y	0.0	0.2554	0.197	0.031
$\sigma(y)$	0.0	0.0004	0.004	0.004
z	0.0	0.3512	0.112	0.407
$\sigma(z)$	0.0	0.0004	0.004	0.004
B	0.3	0.6	0.0	0.0
$\sigma(B)$	0.2	0.06	—	—

similar features of the γ-phase structure ($Zr_5Sc_2O_{13}$) (*3*), with reference to the coordination polyhedra shown in Figs. 2 and 3.

All structures are derived from the parent fluorite cubic structure by a rhombohedral distortion along one of the [111] cubic directions with all the vacant oxygen sites on the threefold rotation axes. All oxygens are missing from these axes in the δ phases, and half the oxygens are missing in the γ-phase structure in such a way as to make the metal atoms on the axis alternately 6- and 8-coordinated.

The position of atoms relative to the ideal fluorite positions can be justified on electrostatic and steric principles. An examination of the bond lengths and angles associated with the coordination of the vacant oxygen site (Fig. 3), as shown in the last part of Table IV, indicates a consistent lengthening of the metal–metal bonds and shortening of the oxygen–oxygen bonds for all phases. In a normal cubic fluorite arrangement these distances would both be 3.7–3.8 Å. It is as though the neighboring oxygens have been drawn in towards this unique *hole* while the metal atoms have been repelled by it. This is consistent with an ionic model for these crystal structures.

Another feature common to all of the structures is the shape of the coordinating polyhedron of the special 6-coordinated metal atom (Metal 1 in Fig. 2). In each case the metal to oxygen distances have become shorter (M–O distance of fluorite ~2.25 Å), and the oxygen to metal to oxygen angle, which is normally the 70.4° associated with the intersection of the diagonals of a cube, is 10° greater and might be considered as tending towards 90° as found for a regular octahedral coordination. This type of coordination is fully defined by the metal to oxygen distance and the O–M–O angle because the metal is on an inversion centre and threefold rotation axis. The *C*-type rare-earth structure, possessed by Sc_2O_3, Y_2O_3, Yb_2O_3, Lu_2O_3, and others, and which may be considered as one end member of

TABLE II

OBSERVED AND CALCULATED STRUCTURE FACTORS FOR THE LOW-TEMPERATURE δ PHASE $Zr_3Yb_4O_{12}$

h k l	F_{obs}	F_{calc}	h k l	F_{obs}	F_{calc}	h k l	F_{obs}	F_{calc}
0 0 3	999.0	955.8	1 −3 1	991.0	1014.5	2 3 5	228.0	231.2
0 0 6	526.0	551.5	1 3 1	211.0	207.2	2 4 1	294.0	253.4
0 −1 1	31.0	34.6	−1 3 2	756.0	759.5	2 4 −2	368.0	307.0
0 1 2	106.0	115.3	1 3 −2	89.0	42.2	2 4 4	210.0	106.6
0 −1 4	226.0	215.1	1 −3 4	944.0	919.8	2 4 −5	262.0	246.3
0 1 5	149.0	168.2	1 3 4	174.0	279.4	2 5 0	135.0	162.8
0 −1 7	123.0	120.4	1 −3 5	659.0	568.9	2 −5 1	99.0	115.3
0 1 8	221.0	230.9	1 −3 7	466.0	476.4	−2 5 2	318.0	348.0
0 2 1	45.0	62.7	1 3 7	289.0	293.4	2 5 −3	327.0	327.6
0 −2 2	48.0	57.3	1 4 0	971.0	930.6	2 5 3	136.0	58.7
0 2 4	166.0	177.3	−1 4 1	143.0	126.9	2 −5 4	71.0	101.5
0 −2 5	175.0	193.9	1 −4 2	194.0	189.4	−2 5 5	352.0	363.2
0 2 7	215.0	225.7	1 4 3	779.0	697.3	−2 6 1	704.0	706.0
0 −3 0	74.0	94.1	1 4 −3	779.0	689.3	2 6 −1	74.0	81.6
0 3 3	63.0	66.1	−1 4 4	86.0	177.4	2 −6 2	544.0	591.0
0 −3 3	233.0	241.0	1 4 6	411.0	439.7	2 6 2	108.0	100.5
0 3 6	57.0	30.8	1 4 −6	464.0	434.9	−2 6 4	617.0	661.0
0 −3 6	200.0	234.3	−1 4 7	192.0	175.8	2 −6 5	477.0	537.8
0 −4 1	273.0	262.3	1 −5 0	67.0	21.2	2 −7 0	165.0	154.2
0 4 2	95.0	100.5	1 5 −1	92.0	78.5	2 −7 3	121.0	175.9
0 −4 4	348.0	340.7	1 −5 3	88.0	105.2	−2 7 3	273.0	215.1
0 4 5	102.0	118.0	−1 5 3	124.0	91.1	2 −8 1	77.0	89.7
0 −4 7	197.0	305.2	1 5 5	74.0	73.9	−2 8 2	26.0	33.7
0 5 1	107.0	141.4	1 −5 6	185.0	186.1	3 3 0	205.0	187.7
0 −5 2	48.0	36.6	−1 5 6	240.0	198.5	3 3 3	200.0	207.3
0 5 4	185.0	212.7	1 −6 1	244.0	274.9	3 3 −3	100.0	67.1
0 −5 5	10.0	19.0	1 6 1	56.0	125.2	3 3 6	344.0	192.6
0 −6 0	121.0	124.9	1 6 −2	14.0	35.6	3 3 −6	94.0	58.6
0 6 3	288.0	313.6	1 6 4	130.0	131.6	3 4 −1	65.0	47.7
0 −6 3	30.0	30.5	−1 6 5	110.0	108.0	3 4 2	228.0	231.1
0 −7 1	574.0	544.1	1 7 0	250.0	303.6	3 4 −4	88.0	92.3
0 7 2	547.0	463.9	−1 7 1	110.0	103.8	3 4 5	223.0	265.4
1 1 0	167.0	139.3	1 −7 2	220.0	247.6	3 5 1	487.0	542.9
1 1 3	61.0	28.6	−1 7 4	43.0	21.3	3 5 −2	369.0	458.8
1 1 −3	282.0	261.2	1 −8 0	193.0	136.8	3 −7 1	25.0	38.0
1 1 6	153.0	151.6	2 2 −3	57.0	55.4	−3 7 2	104.0	36.3
1 1 −6	217.0	260.2	2 2 3	63.0	63.0	3 −7 4	32.0	20.1
1 2 −1	122.0	74.7	2 2 6	48.0	74.5	−3 7 5	41.0	47.5
1 2 2	133.0	128.2	2 2 −6	27.0	5.2	−3 8 1	337.0	258.5
1 2 −4	212.0	63.6	2 3 −1	90.0	74.0	3 −8 2	78.0	143.2
1 2 5	375.0	248.6	2 3 2	335.0	221.2	4 4 0	155.0	175.2
1 2 −7	133.0	124.7	2 3 −4	68.0	24.6	4 4 3	209.0	231.7
						4 4 −3	143.0	159.5

the homologous series M_nO_{2n-2}, also has a metal atom site of similar coordination and symmetry. For Sc_2O_3 (*14*) the relevant M–O distance is 2.13 Å and the O–M–O angle is 80.3°, and for In_2O_3 (*15*) these same parameters are respectively 2.18 Å and 80.7°.

Metal Ordering

A comparison of the information available seems to indicate that there are varying degrees of metal-ordering in these structures, while the anion lattice is complete in each case. The controlling feature of

TABLE III

OBSERVED AND CALCULATED STRUCTURE FACTORS FOR THE HIGH-TEMPERATURE δ PHASE $Zr_3Yb_4O_{12}$

h	k	l	F_{obs}	F_{calc}	h	k	l	F_{obs}	F_{calc}	h	k	l	F_{obs}	F_{calc}
0	1	2	24.2	17.9	1	−7	2	7.0	4.3	2	−10	3	56.2	45.3
0	2	1	14.5	10.2	1	7	3	11.1	7.5	3	3	0	23.2	21.0
0	−2	2	8.0	4.1	1	7	−3	21.0	10.6	3	3	3	6.6	3.4
0	2	4	25.8	27.5	−1	7	4	24.5	21.4	3	4	−1	2.4	0.8
0	3	0	19.5	16.8	1	−8	0	38.7	43.8	3	4	2	12.8	9.5
0	3	3	16.1	9.0	1	8	−1	25.0	15.4	3	5	1	28.8	31.2
0	−3	3	31.9	32.3	1	8	2	47.5	39.9	3	5	−2	12.8	13.5
0	−4	1	29.5	26.3	−1	8	3	42.8	38.8	3	5	4	33.5	42.0
0	4	2	10.0	7.0	1	−8	3	60.6	46.7	3	6	0	56.4	66.2
0	−4	4	48.2	41.5	1	−9	1	35.4	23.6	3	6	3	44.1	57.5
0	5	1	14.9	11.5	−1	9	2	15.0	6.4	3	−7	1	8.1	6.8
0	−5	2	3.4	1.8	2	2	0	11.6	6.5	3	7	−1	41.0	36.2
0	5	4	22.4	24.0	2	2	3	5.1	5.4	3	7	2	36.0	34.6
0	6	0	18.1	12.9	2	3	−1	16.3	13.3	−3	7	2	23.9	29.4
0	6	3	30.3	36.7	2	3	2	35.4	37.8	3	−7	4	15.1	16.8
0	−7	1	78.3	70.8	2	4	1	86.9	89.8	3	7	−4	40.1	30.1
0	7	2	55.0	63.9	2	4	−2	83.0	77.5	−3	8	1	63.9	71.6
0	−7	4	63.7	64.4	2	4	4	81.6	83.3	3	−8	2	58.4	63.4
0	8	1	28.5	21.2	2	5	0	25.1	26.4	3	−9	0	8.2	1.7
0	−8	2	37.7	28.0	2	−5	1	18.9	15.3	−3	9	3	16.4	1.5
0	8	4	23.8	17.2	−2	5	2	27.7	29.2	3	−9	3	19.3	9.6
0	9	0	10.3	5.4	2	5	3	31.4	30.3	3	−10	1	24.9	18.0
0	9	3	17.5	11.4	2	−5	4	4.6	0.9	−3	10	2	27.0	24.4
1	2	−1	106.7	121.3	−2	6	1	29.6	36.6	3	−10	4	13.6	12.8
1	2	2	89.2	95.3	2	6	−1	8.1	7.6	4	4	0	23.2	25.7
1	−2	3	34.7	29.4	2	6	2	6.7	2.8	4	4	3	21.5	19.5
1	3	1	29.0	24.1	2	−6	2	37.4	43.7	4	5	−1	19.4	17.6
1	−3	1	10.0	3.9	2	6	−4	20.2	13.3	4	5	2	9.3	5.5
−1	3	2	9.2	7.9	2	−7	0	21.6	20.4	4	6	1	4.7	3.7
1	3	−2	26.4	27.6	2	7	1	47.2	42.4	4	6	4	6.3	3.4
1	3	4	28.0	27.3	2	7	−2	51.7	48.1	4	7	0	18.5	16.9
1	−3	4	13.5	13.4	2	−7	3	34.6	39.0	4	7	−3	5.9	0.4
1	4	0	2.8	3.1	2	7	4	31.1	32.4	4	−9	1	35.7	44.5
−1	4	1	21.5	20.5	2	8	0	26.5	15.1	−4	9	2	31.1	45.3
1	−4	2	4.8	3.3	2	−8	1	14.4	9.6	4	−9	4	38.6	39.7
1	4	3	19.5	17.3	−2	8	2	13.3	8.4	−4	10	1	21.5	15.2
1	−5	0	110.4	116.0	2	8	3	4.4	0.7	4	−10	2	36.0	36.0
1	5	−1	33.1	38.1	2	8	−3	31.8	23.5	−4	10	4	11.9	8.5
1	5	2	32.9	34.1	2	−8	4	6.5	3.6	4	−11	0	21.4	13.1
1	−5	3	80.3	92.4	−2	9	1	28.8	24.6	5	5	0	9.0	6.5
1	6	1	15.3	12.5	2	−9	2	14.6	12.0	5	5	3	4.1	3.8
1	−6	1	19.6	14.3	−2	9	4	36.5	31.2	5	6	−1	43.4	33.1
1	6	−2	27.8	25.5	2	−10	0	64.0	52.3	5	11	1	52.2	45.0
1	6	4	6.5	5.5	−2	10	3	64.4	48.8	−5	11	2	52.4	44.9
1	7	0	16.5	14.7										

the cation ordering appears to be the relative sizes of the cations and not the relative charges. UY_6O_{12} and ULu_6O_{52} (*18*) are completely ordered structures and have the smaller more highly charged uranium atoms occupying the site of lesser volume and lower coordination. The low-temperature form of $Zr_3Yb_4O_{12}$ has the cations partially ordered in that there is a distinct preference to have the smaller more highly charged zirconium atom occupying the special 6-coordinated atom position: the approximate ratio is 3 Zr atoms in that position to every one Yb atom. The remaining Yb and Zr atoms are

TABLE IV

BOND LENGTHS AND ANGLES FOR δ PHASES[a]

	$Zr_3Sc_4O_{12}$	$Zr_3Yb_4O_{12}$ H.T.	$Zr_3Yb_4O_{12}$ L.T.	UY_6O_{12}	ULu_6O_{12}	$Zr_{10}Sc_4O_{26}$
Polyhedron around M(I)						
M(I)–O(I)	2.13 Å	2.07	2.03	2.07	2.08	2.13
σ	0.01	0.06	0.04	0.03	0.05	0.02
O(I)–O(I′)	2.74	2.56	2.68	2.81	2.81	2.73
σ	0.02	0.09	0.05	0.03	0.05	0.03
O(I)–M(I)–O(I′)	79.9°	76.6	82.7	85.3	84.7	80.0
σ	0.4	2.2	1.6	1.0	1.0	0.6
Polyhedron around M(2)						
M(II)–O(I)	2.08 Å	2.32	2.22	2.31	2.27	2.08
M(II)–O(I′)	2.55	2.55	2.59	2.78	2.77	2.05
M(II)–O(I″)	2.03	2.08	2.26	2.40	2.30	2.20
M(II)–O(II‴)	2.27	2.44	2.21	2.30	2.25	2.11
M(II)–O(II)	2.07	2.03	2.16	2.17	2.15	2.28
M(II)–O(II′)	2.22	2.27	2.26	2.28	2.24	2.27
M(II)–O(II″)	2.08	2.26	2.24	2.29	2.25	2.10
σ	0.01	0.06	0.05	0.03	0.05	0.02
O(I)–O(II)	3.12	3.14	3.22	3.23	3.17	
O(I)–O(I′)	2.70	2.89	2.79	2.91	2.87	
O(I)–O(II′)	2.61	2.92	2.77	2.86	2.77	
O(I)–O(II″)	3.00	3.19	3.27	3.31	3.24	
O(II)–O(I′)	2.75	2.69	2.96	3.03	2.96	
O(II)–O(II‴)	2.62	2.85	2.58	2.80	2.74	
O(II)–O(II″)	3.18	3.28	3.39	3.58	3.49	
O(I′)–O(I″)	2.74	2.56	2.68	2.81	2.81	
O(I″)–O(II′)	2.75	2.69	2.96	3.03	2.96	
O(I″)–O(II‴)	2.61	2.92	2.77	2.86	2.77	
O(II″)–O(II′)	2.61	2.80	2.79	2.83	2.83	
O(II″)–O(II‴)	2.62	2.85	2.58	2.80	2.74	
σ	0.02	0.06	0.06	0.03	0.05	
O(I)–M(II)–O(I′)	70.4°	72.8	70.4	69.0	68.4	
O(I)–M(II)–O(II′)	74.6	79.2	76.3	77.2	76.2	
O(II)–M(II)–O(I)	72.1	71.0	76.8	74.4	72.9	
O(II)–M(II)–O(II‴)	74.0	78.9	72.5	77.4	77.0	
O(I′)–M(II)–O(I″)	72.6	66.5	66.8	65.3	66.5	
O(I″)–M(II)–O(II′)	80.6	76.3	82.0	80.8	81.5	
O(I″)–M(II)–O(II‴)	74.4	80.2	76.7	75.0	75.6	
O(II″)–M(II)–O(II′)	74.7	76.4	76.7	76.7	78.1	
O(II″)–M(II)–O(II‴)	73.8	74.7	70.8	75.1	75.0	
σ	0.6	2.0	1.5	0.6	0.8	
Polyhedron around vacant site						
M(I)–M(II)	3.761 Å	3.905	3.907	4.063	4.021	3.800
M(II)–M(II)	3.819	3.990	3.962	4.005	3.980	4.047
σ	0.004	0.005	0.004	0.004	0.005	0.004
O(I)–O(I)	3.27	3.25	3.05	3.05	3.08	2.73
O(I)–O(II)	3.00	3.19	3.27	3.31	3.24	2.99
O(II)–O(I)	3.12	3.14	3.22	3.23	3.17	3.35
O(II)–O(II)	3.18	3.28	3.39	3.58	3.49	3.12
σ	0.02	0.06	0.06	0.03	0.05	0.03

[a] Those for the γ phase $Zr_{10}Sc_4O_{26}$ are included where the polyhedra are similar.

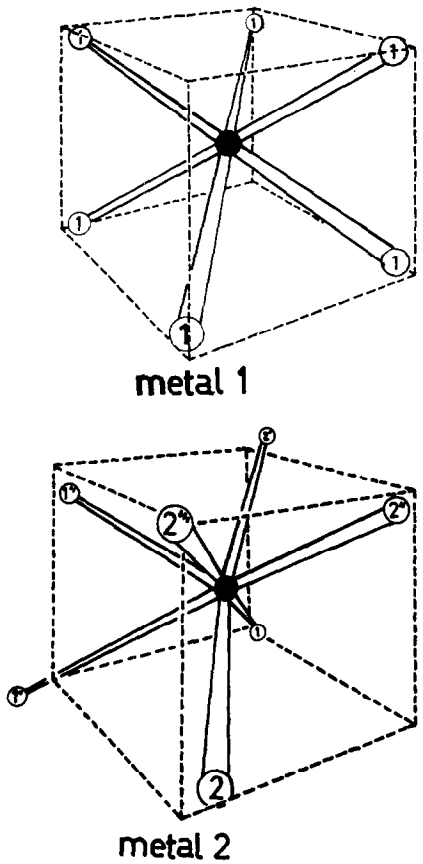

FIG. 2. Coordination polyhedra of the metal atoms for the δ phases.

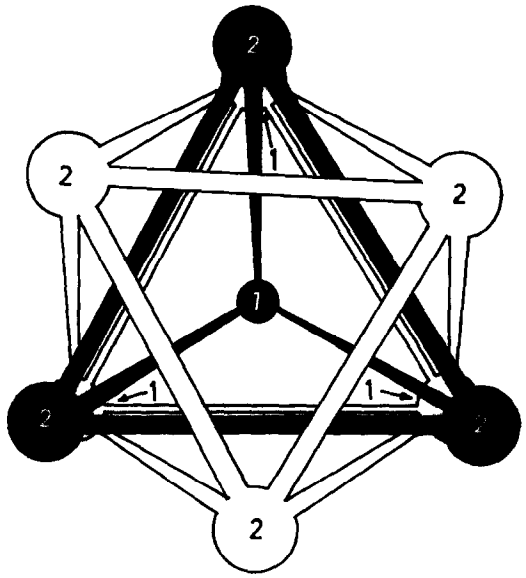

FIG. 3. Immediate surroundings of the special unoccupied oxygen site.
Black tetrahedron—neighbouring metal atoms.
White octahedron—neighbouring oxygen atoms.

disordered over the remaining general site. Probably the true equilibrium structure would have all the special metal sites occupied by Zr atoms. This *tolerance* the structure has for allowing some Yb atoms into these special positions is a likely reason for the ready formation of this low-temperature phase in the ZrO_2–$YbO_{1.5}$ system at temperatures where cation diffusion may not be all that great. The high-temperature $Zr_3Yb_4O_{12}$ phase has been shown to have a disordered cation lattice, as do $Zr_{10}Sc_4O_{26}$ and $Zr_3Sc_4O_{12}$. This suggests that the size discrepancy between the Zr and Yb atoms is really tolerated by the structure at high temperatures only, whereas the sizes of Zr and Sc atoms are so similar that these atoms show no site preference, even at low temperatures.

The length of the M(II)–O(I′) bond for all the δ-phase structures is longer than 2.5 Å whereas most other M–O bonds do not deviate much from 2.2 Å (Table IV). This bond distance is longer for the UY_6O_{12}, ULu_6O_{12}, and $Zr_3Yb_4O_{12}$ (low-temperature) structures, where the metal atoms are ordered, than for those with disordered metal atoms [$Zr_3Sc_4O_{12}$ and $Zr_3Yb_4O_{12}$ (high-temperature)], and may result from this increase in metal-ordering. In the ordered structures the more highly charged cation is occupying the position of lower coordination. Charge balance is probably maintained by these coordinating oxygens approaching nearer to this cation, and thus the contribution these oxygens are making to the coordination of the cation with the lesser charge is diminished.

References

1. D. J. M. BEVAN AND J. KORDIS, *J. Inorg. Nucl. Chem.* **69**, 480 (1964).
2. D. J. M. BEVAN, W. W. BARKER, R. L. MARTIN, AND T. C. PARKS, "Rare Earth Research," (L. Eyring, Ed.), Vol. 3, p. 441, Gordon and Breach, New York, 1965.
3. M. R. THORNBER, D. J. M. BEVAN, AND J. GRAHAM, *Acta Cryst.* **B24**, 1183 (1968).
4. A. D. WADSLEY, *Rev. Pure Appl. Chem.* **5**, 165 (1955).
5. S. M. ARIYA AND YU. G. POPOV, *J. Gen. Chem. Moscow* **32**, 2077 (1962).
6. J. S. ANDERSON, *Advan. Chem.* **39**, 1 (1963).
7. A. D. WADSLEY, *Advan. Chem.* **39**, 23 (1963).
8. B. G. HYDE, D. J. M. BEVAN, AND L. EYRING, *Phil. Trans. Roy. Soc. A* **259**, 583 (1966).
9. M. PEREZ Y JORBA, *Ann. Chim.* **8**, 117 (1963).
10. A. I. M. RAE AND W. W. BARKER, *Acta Cryst.* **14**, 1208 (1961).

11. B. N. FIGGIS, "Programs for the Inclined Beam Oscillation Technique," University of Western Australia.
12. W. R. BUSING, K. O. MARTIN, AND H. A. LEVEY, Oak Ridge National Laboratory, Report No. ORNL-TM-305 (1962).
13. S. F. BARTRAM, *Inorg. Chem.* **5**, 749 (1966).
14. S. GELLER, P. ROMO, AND J. P. REMEIKA, *Z. Krist.* **124**, 137 (1967); *Z. Krist.* **126**, 461 (1968) errata.
15. M. MANEZIO, *Acta Cryst.* **20**, 723 (1966).